Korean J. Chem. Eng., **31**(10), 1810-1817 (2014)
DOI: 10.1007/s11814-014-0103-6

pISSN: 0256-1115
eISSN: 1975-7220

Optimization of preparation conditions of activated carbon from the residue of desilicated rice husk using response surface methodology

Xiuli Han*,†, Yuyuan He*, Haohao Zhao*, and Duo Wang**

*School of Chemical Engineering and Energy, Zhengzhou University,
Kexue Road 100#, Zhengzhou, Henan 450001, P. R. China
**State Key Laboratory of Motor Vehicle Biofuel Technology, Nanyang 473000, P. R. China
(*Received 8 November 2013 • accepted 8 April 2014*)

Abstract−Activated carbon could be prepared from residue of rice husk using physical activation with steam as activating agent. Response surface methodology (RSM) was applied to optimize the effects of processing parameters, and regression analysis was performed on the data obtained. The optimal conditions for adsorption capacity of activated carbon from the residue of rice husk were activation temperature of 946 °C, activation time of 31 min and water (18 g) which changed to steam by heating, resulting in 970.06 $mg \cdot g^{-1}$ of iodine adsorption capacity and 31.36% of activated carbon yield. The activated carbon prepared under optimum condition was mesoporous with BET surface area of 1,004.296 $m^2 \cdot g^{-1}$, total pore volume of 0.9388 $cm^3 \cdot g^{-1}$ and average pore diameter of 2.043 nm. The surface chemical functional groups of activated carbon were identified by FT-IR, and its microstructure was examined by scanning electron microscopy (SEM). We concluded that the process of physical activation with steam could be an environmentally harmonious and effective method for preparing activated carbon from residue of desilicated rice husk.

Keywords: Rice Husk, Steam, Activated Carbon, Response Surface Methodology

INTRODUCTION

Activated carbon is a carbonaceous adsorbent that has been widely used in chemical reactions as catalyst support, in medicine as medical adsorbent [1], and in electric double-layer capacitors as electrode due to its high adsorption. The adsorption properties of activated carbon are strongly considered in the activation process and nature of source materials [2]. Usually, the specific surface area of activated carbon ranges from 500 to 3,000 $m^2 \cdot g^{-1}$, and adsorption properties of activated carbon depend strongly on their complex network pores, especially contributions of micropores (diameters<2 nm), mesopores (2 nm<diameters<50 nm), and macropores (diameters >50 nm) [3].

Activated carbon is usually prepared by chemical activation or physical activation method, respectively, using a chemical reagent, such as sodium hydroxide, potassium carbonate or phosphate and steam or carbon dioxide as activator. The chemical activation method is that raw materials are impregnated at high temperatures with chemical reagent, carbonization and activation completed at once. The physical activation method involves carbonization of raw materials at the temperatures between 400 °C and 600 °C in a furnace under inert atmosphere, and then the char is activated by activating agents such steam or CO_2 in furnace [4,5]. The research reported is that activated carbon activated by steam has a narrower and more extensive microspore system than by carbon dioxide; the larger molecular dimensions of the CO_2 would make more difficult and slower when it goes through the pore of the carbon materials than H_2O [6-8]. In addition, chemically activated carbon has plenty of inorganic content, which may cause environmental contamination. So physical activation is more favorable than chemical activation to obtain cleaner production [9].

Almost activated carbon can be produced by carbonaceous materials, such as oil palm fiber [10], paper mill sludge [11], coal [12], wood [13] and so on. In industrial practice, coal is the main source for the production of activated carbon. Since coal is a non-renewable fossil oil resource, the coal would be replaced by the natural, renewable and low-cost materials. Biomass, as a kind of widely renewable energy source, has become a hot point for studying, such as olive bagasse [14], eucalyptus and wattle wood [15], almond shell [16] and so on [17-19]. Rice husk, one of biomasses, is the main by-product in rice processing. Currently, about of 40 million tons of rice husk are produced in China every year as residue [20]. The rice husk contains three main components: cellulose, lignin and mineral components. It has the advantage of producing activated carbon, because of high cellulose and lignin content of rice husk [21]. The main elements of residue left are carbon and silica after rice husk is used in a pyrolysis experiment, so it is also an advantageous material to produce silica white [22]. However, a large amount of solid residue which produced silica white was left. If not utilized properly, the residue will become a tremendous waste. The residue could be used to produce activated carbon because it has low ash content. In addition, it is chosen to apply as precursor due to granular structure, chemical stability, high mechanical strength and its local availability low-cost mostly [23].

In present work on preparation, an activated experiment of residue desilicated rice husk is carried out with steam as activating agent under activation temperature, to obtain high adsorption capacity using RSM which optimizes the conditions of preparation. The NOVA

†To whom correspondence should be addressed.
E-mail: xlhan@zzu.edu.cn, heyuyuan0619@163.com
Copyright by The Korean Institute of Chemical Engineers.

Table 1. Proximate and ultimate analysis of CRH and DRH (wt%)

Analysis	CRH	DRH
Ultimate		
Carbon	52.84	78.43
Nitrogen	0.41	0.7
Hydrogen	1.52	2.12
Proximate		
Silicon dioxide	36.71	2.78

200e of surface area and pore size analyzer is used to describe characterization specific surface area and pore size distribution.

MATERIALS AND METHODS

1. Materials

The rice husk residue was collected from the local silica manufacturer. Rice husk was placed into a pyrolysis furnace at high temperature without air; a char called carbonization rice husk (CRH) was left. And then the char was boiled with sodium carbonate solution in the reaction still under high pressure. The char was immediately washed with hot water; the filtrate could be used to produce silica white and the residue of desilicated rice husk (DRH) was used to produce activated carbon as the precursor.

The proximate and ultimate analysis of the CRH and DRH used in this study are given in Table 1. The contents of C, H and N elements in the ultimate analysis were determined by an elemental analyzer (1112series, Thermo Electron Corporation). The analytical results shown in Table 1 reveal that DRH has high carbon and low silicon dioxide content, indicating that this precursor is suitable for the preparation of activated carbon.

2. Activation

In the activation step, a precursor of 6 g was loaded into the steel pipe with inner diameter of 18 mm; the steel pipe was inserted inside horizontal furnace and heated from room temperature to activation temperatures that were 850 ºC, 900 ºC and 950 ºC, respectively, with heating rate of 8 ºC·min^{-1}. When activation temperature was reached and nitrogen flow was rapidly substituted by flowing steam, the flowing steam was provided by injection liquid water which passed through a coil inserted in another electrical furnace; the amount of water was 6 g, 12 g and 18 g, respectively. In furnace activation contacting for 15 min, 30 min and 45 min, steam was kept constant for the desired period of activation with precursor. At the end of activation period, steam was switched to nitrogen flowing until the sample was cooled to room temperature, so that oxygen from air did not burn off activated carbon [24].

3. Iodine Adsorption

Activated carbon was crushed to a size of 0.074 mm; a dose of activated carbon was put into 250 mL Erlenmeyer flask with ground glass stopper. The dose was well dispersed in 10 mL of 3.23 mol·L^{-1} HCl solution in flask, and then the mixture was simmered for thirty seconds. After being cooled to room temperature, 50 mL of 0.1 mol·L^{-1} iodine solution was poured to an Erlenmeyer flask, and the flask was shaken at 240-275 rpm in rotary shaker at room temperature for 15 min. The reacted solution was immediately filtered in dry conical flask with glass core funnel of G3. Accurately, 10 mL of filtrate and 100 mL distilled water were titrated analyzed with standardized 0.1 mol·L^{-1} sodium hyposulfite in a conical flask. Adsorption capacity and yield of activated carbon were calculated using following formula:

$$Q_t=[5(10C_1-1.2C_2V_1)\times 127\times D]/m \quad (1)$$

$$Y=m/m_0\times 100\% \quad (2)$$

where Q_t is the adsorption capacity (mg·g^{-1}), C_1 is the concentration of the iodine standard solution (mol·L^{-1}), C_2 is the concentration of sodium hyposulfite standard solution (mol·L^{-1}), V_1 is the consumption of sodium hyposulfite solution (mL), m is the weight of activated carbon (g), 127 is the molar mass of iodine (0.5 I_2, g·mol^{-1}), D is the correction factor, Y is the yield of activated carbon (%), m_0 is the weight of precursor (g).

RESULTS AND DISCUSSION

1. Optimization of Experiment Conditions for Activated Carbon Produced

RSM is a statistical and mathematical technique which uses quantitative data from experiments to confirm regression model equations and operating conditions, so it is useful for improving, developing and optimizing a process. In this work, we chose activation temperature, activation time and the amount of water based on literature and preliminary studies as given in Table 2. A three-level full factorial design was used for development of activated carbon production to obtain the relation between iodine adsorption capac-

Table 2. Independent variables and their coded levels for the central composite design

Factors	−1	0	1
X_1: Temperature (ºC)	850	900	950
X_2: Time (min)	15	30	45
X_3: Water (g)	6	12	18

Table 3. Experimental design matrix for preparation of activated carbon

Run	X_1 (ºC)	X_2 (min)	X_3 (g)	Q_t (mg·g^{-1})	Y (%)
1	850	15	6	588.05	78.27
2	950	15	12	799.05	54.59
3	850	45	12	782.48	66.67
4	950	45	12	845.43	33.73
5	850	30	6	655.8	74.01
6	950	30	6	865.73	59.67
7	850	30	18	786.31	63.56
8	950	30	18	973.32	31.77
9	900	15	6	674.17	73.98
10	900	45	6	719.13	69.58
11	900	15	18	842.08	55.59
12	900	45	18	901.46	43.32
13	900	30	12	858.71	60.16
14	900	30	12	876.01	59.23
15	900	30	12	878.85	59.26

Table 4. Analysis of variance for selected factorial model for adsorption capacity

Source	Sum of squares	DF	Mean square	*F*-value	Prob.>F	Status
Model	1.463E+005	9	16260.28	13.49	0.0052	Signification
X_1	56261.67	1	56261.67	46.66	0.0010	
X_2	14891.07	1	14891.07	12.35	0.0170	
X_3	43267.99	1	43267.99	35.89	0.0019	
X_1X_2	5479.70	1	5479.70	4.54	0.0862	
X_1X_3	131.33	1	131.33	0.11	0.7547	
X_2X_3	51.98	1	51.89	0.043	0.8437	
Lack of fit	5790.75	3	1930.25	16.24	0.0585	Not significant
Residual	6028.41	5	1205.68			
Pure error	237.66	2	118.83			
Cor total	1.524E+005	14				

ity and yield.

To obtain optimization of the physical condition of activated carbon, we designed the experiment project with response surface methodology in Table 3. The optimum activation condition of activation carbon was obtained by the developed regression model for improvement of adsorption capacity ($mg \cdot g^{-1}$) and activated carbon yield (%). The final model equation for iodine adsorption was as follows:

$$Q_t=871.19+83.36X_1+43.14X_2+73.54X_3-37.01X_1X_2-5.73X_1X_3 +3.60X_2X_3-40.68X_1^2-76.76X_2^2-10.22X_3^2 \quad (3)$$

where Q_t is the iodine adsorption capacity in $mg \cdot g^{-1}$, X_1 is the activation temperature in °C, X_2 is the activation time in minutes and X_3 is the amount of water in g.

Coefficients with one factor represent the effect of particular factor, and the coefficients with two factors, and those with second-order terms, respectively, represent interaction between two factors and quadratic effect. The performance of models developed was evaluated based on correlation coefficients, R^2 value. In fact, the models developed seem to be best at low standard deviation and high R^2 statistics, which was closer to unity as it would give predicted value closer to actual value for responses [25]. In this experiment, the R^2 value for Eq. (3) was 0.9604. This indicated that 0.9604 of total variation in activated carbon adsorption capacity was attributed to the experimental variables studied. The R^2 value of 0.9604 for Eq. (3) was considered relatively high, indicating that predicted values for adsorption capacity would be more accurate and closer to its actual value.

The adequacy of the model was justified through analysis of variance for response of activated carbon's adsorption capacity. Values of 'Prob>F' less than 0.05 implies that model terms are significant. In Table 4, the 'Prob>F' value was 0.0052, indicating that the model was significant. The result also indicated that activation temperature was highly significant since its 'Prob>F' value was 0.0010. Therefore, it had a major effect on adsorption properties of activated carbon produced. Activated time has less effect on adsorption capacity of activated carbon produced that its 'Prob>F' value was 0.0170. The 'lack-of-fit *F*-value' was a portion of residual sum of squares that was due to model not fitting data [26]. As can be seen from Table 4, the 'lack-of-fit *F*-value' of 16.24 implies that there is not signification curvature (as measured by difference between the average of center points and factorial points) in design space.

Table 5. Standard deviation and R^2 for the model Eq. (3)

Std. Dev.	34.72	R-squared	0.9604
Mean	803.11	Adj R-squared	0.8892
C.V. %	4.32	Pred R-square	0.3884
Press	93186.69	Adeq precisior	13.482

Predicted adsorption capacity values from equation are given in Table 3. The value of the determination coefficient (R^2=0.9604) for Eq. (3) indicates that about 3.96% of total variations were not satisfactorily explained by the model in Table 5. The analysis of variance in Table 4 could be used to test statistical significance of ratio of mean square due to regression and mean square due to residual error.

Fig. 1 shows theoretical versus experimental values for adsorption capacity by Eq. (3). The theoretical values obtained are quite close to experimental values, indicating that the model developed was successful in capturing the correlation between activated carbon preparation variables to adsorption capacity. Quality of the model developed was evaluated based on coefficient of determination value. The experimental values of both responses are matched well with

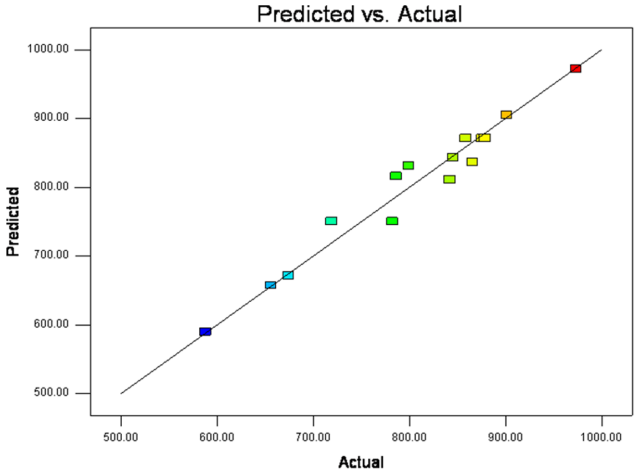

Fig. 1. Theoretical vs. experimental adsorption capacity of iodine values of the activated carbon.

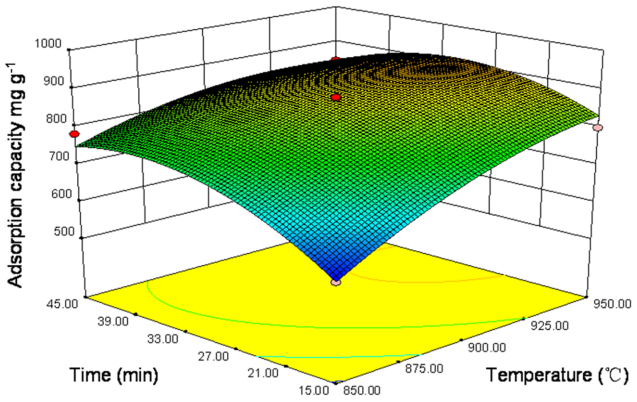

Fig. 2. Three-dimensional response surface plots: Effect of activation temperature and time on adsorption capacities of the activated carbon.

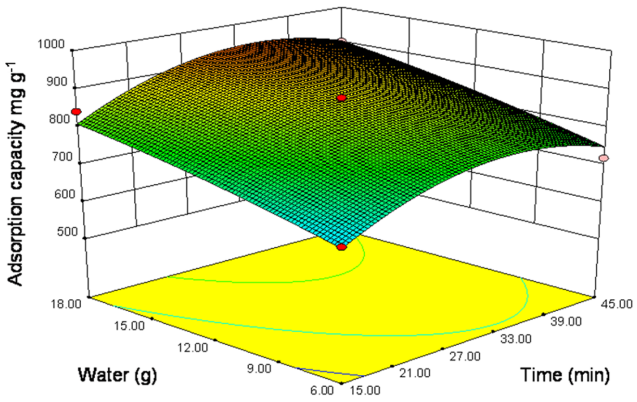

Fig. 4. Three-dimensional response surface plots: Effect of activation of activation time and the amount of water on adsorption capacities of the activated carbon produced.

theoretical responses.

Figs. 2-4 show the results of fitting experimental iodine adsorption data to response model represented by Eq. (1). Due to surface area and pore size of activated carbon, the adsorption capacity was its most important characteristic. As can be observed from Fig. 2, the three-dimensional response surface of combined effect of activation temperature and activation time on iodine value shows that the iodine value of activated carbon increases with the increases activation temperature, and iodine value of activated carbon increases and decreases with increases the activation time. Leading to a change in activation energy for activation reaction, if changing in activation temperature and time happened, this would affect the rate of reaction for variety of conversion, so that the result indicated modifications in carbon porous structure [27].

Fig. 3 shows the three-dimensional response surface of combined effect of activation temperature and the amount of water on iodine value. The adsorption capacity of iodine decreases with decreasing activation temperature and amount of water. The change in the amount of water and activation temperature leads to a change in the activation energy for steam-carbon reaction, which would influence the reaction rate for the variety of conversion; the change in conversion is indicative of modifications in the activated carbon porous structure [28]. The adsorption capacity is directly affected by the

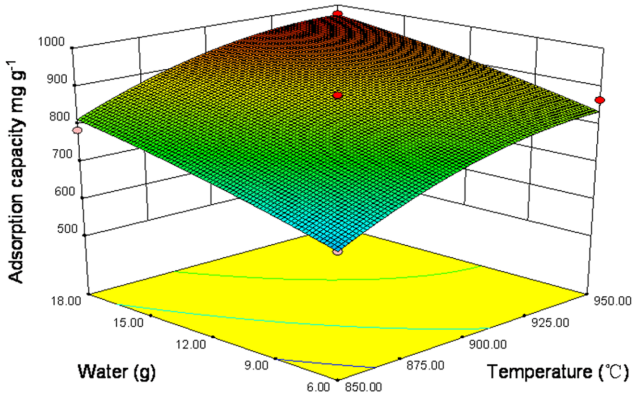

Fig. 3. Three-dimensional response surface plots: Effect of activation temperature and the amount of water on adsorption capacities of the activated carbon produced.

porous nature of activated carbon decided by the internal surface area, so the adsorption capacity increased with an increase in the activation temperature and the amount of water. From Fig. 4, the 3D response surface of combined effect of activation time and amount of water on adsorption capacity, iodine value of activated carbon increases with increases amount of water, and the adsorption capacity increases and then decreases with increased activation time. So the adsorption capacity of iodine reaches a maximum value in activation time of 22.5-37.5 min.

From Figs. 2-4, the results clearly show that the interaction effect between activation temperature and activation time is greater than activation temperature and amount of water. The interaction effect between activation time and amount of water had little influence. From RSM, it has been seen that activation temperature had greater effect with *F*-value of 46.66 than amount of the water with *F*-value of 35.89, and activation time had little effect with *F*-value of 12.35. The amount of water was a significant parameter affecting adsorption capacity of activated carbon [29]. It can been said that activation temperature and amount of water are the most important parameters for producing activated carbon in accordance with a previous report [30].

The yield of activated carbon is also an important parameter as its adsorption capacity. Yield and adsorption capacity had somewhat of a reverse relationship. Loss of activated carbon yield was due to the reaction between water molecules and carbon element at high temperature, primary to the increase of pore development and creating of new pores with following chemical reaction equations [31,32]:

$$H_2O(g)+C(s)\rightarrow CO(g)+H_2(g)$$
$$H_2O(g)+C(s)\rightarrow CO_2(g)+H_2(g)$$

However, over-activation might lead to a large number of carbon atoms reducing and enlarging the aperture; the resulting would have been the adverse effect of reducing surface area and activated carbon yield [33]. When the activator came in contact with precursor at the initial activation, the amorphous components in the exterior and the interior of the precursor were removed; meanwhile, the crystallitic carbon was activated with the activator and the crystallitic matter was burnt-off at high activation temperatures. So the yield of activation carbon was decreased [34]. This is similar to the report

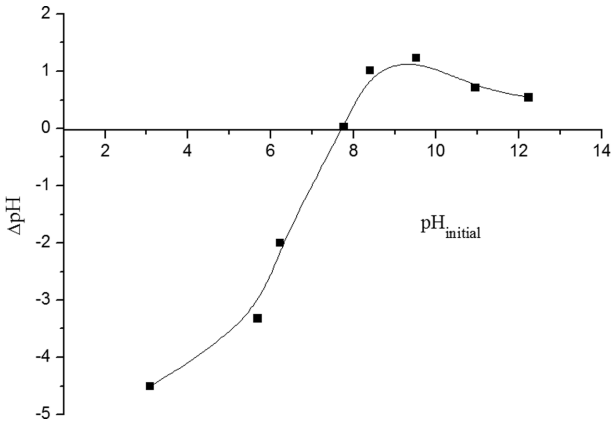

Fig. 5. The point of zero charge of activated carbon.

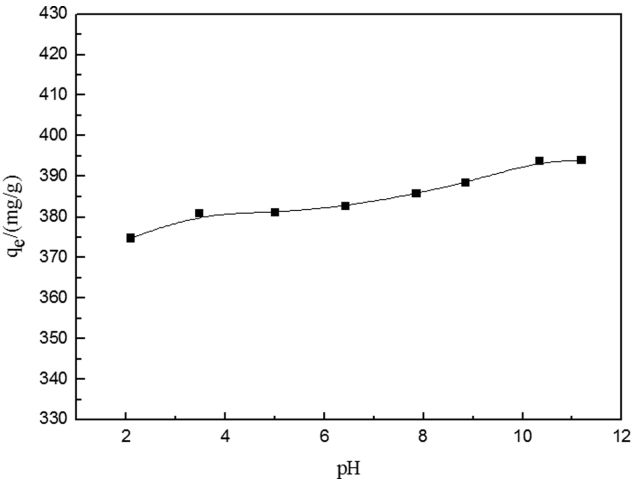

Fig. 6. Effect of initial pH for adsorption of MB onto the activated carbon.

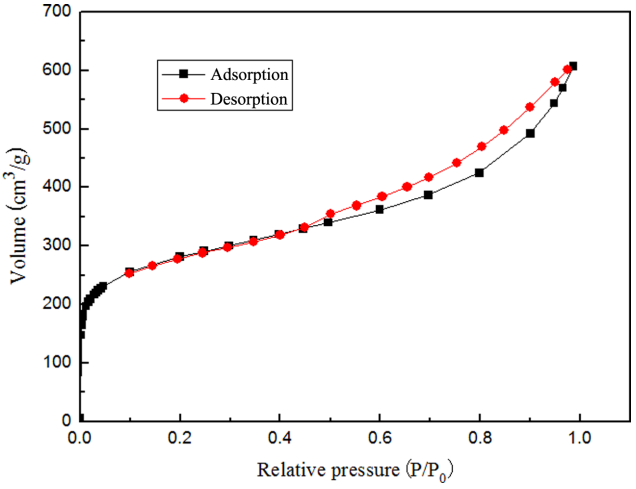

Fig. 7. Nitrogen adsorption isotherm of the activated carbon.

that the microporous of apricot stones corresponds to a more widened porous structure as the burn-off increases [35].

2. Process Optimization

Adsorption capacity and yield are the most important properties of activated carbon. Both of properties have an opposite relationship with process parameters, yet adsorption capacity is the main object of study. Based on experimental results, optimization of prepared parameters of activated carbon was carried out using RSM. Taking Eq. (3) for the partial derivatives of independent variables, then equations solved to obtain the optimum operating conditions calculated were activation temperature of 946.14 °C, activation time of 31.24 min and the water amount of 18 g. According to actual situations and experimental convenience, the experimental conditions which were temperature of 946 °C, time of 31 min and water amount of 18 g were chosen to produce activated carbon. Activated carbon was produced under the optimized conditions. Iodine adsorption capacity of activated carbon under optimum activation conditions was 970.06 mg·g^{-1}, which was predicted by model to be 972.48 mg·g^{-1}, and the yield of activated carbon was 31.36%. The experimental values obtained were in good agreement with values predicted from the model.

3. Methylene Blue Adsorption

Methylene blue (MB) is used as adsorbate to determine the adsorption capacity of activated carbon. Adsorption experiments were performed by using a sample containing 1 g·L^{-1} of activated carbon and 20 mL of MB solution with initial concentration of 400 mg·L^{-1} in 50 mL flasks. The flasks were shaken on a mechanical shaker at 100 rpm for 240 min at 298 K. After shaking, the adsorbent-dye mixtures were separated from solution by centrifugation and the supernatants were analyzed by a spectrophotometer (WFZ UV-2012PC) at 665 nm to determine the residual concentration.

The point of zero charge (pH$_{pzc}$) of an adsorbent is a very important characteristic that determines the pH at which the surface charge is zero. The pH$_{pzc}$ determination of the activated carbon was performed according to the solid addition method [36]. The adsorbent surface has a net positive charge for pH<pH$_{pzc}$, while the adsorbent has a net negative charge for pH>pH$_{pzc}$. The pH$_{pzc}$ of activated carbon is shown in Fig. 7, from the results it was between 7.5 and 8.0.

Initial pH value of MB solution is one of the most important factors influencing the adsorption. The initial solution pH was adjusted using 0.1 mol·L^{-1} HCl or 0.1 mol·L^{-1} NaOH. Fig. 6 shows the effect of pH on the adsorption of MB. The pH of initial solution was near 7, and the adsorption capacity of activated carbon for MB was 382.65 mg·g^{-1} in the original. This figure indicates that the adsorption capacity of activated carbon for MB increased from 374.77 mg·g^{-1} to 393.87 mg·g^{-1} with increasing pH from 2.1 to 11.2. The activated carbon is more negatively charged when pH>pH$_{pzc}$, which provided more binding sites of activated carbon to attract MB cations due to electrostatic attraction. Therefore, there is lower adsorption at lower pH because of the presence of H ions competing with the cations for surface of activated carbon; on the contrary, strengthening electrostatic attractions between MB$^+$ ions and negatively charged adsorption sites causes an increase adsorption capacity of MB [37]. However, because of the slight change of adsorption capacity at the pH range of 2.1-11.2, the mechanism for MB adsorption is not only an electrostatic mechanism but also has a chemical reaction mechanism.

The comparison of adsorption capacities of activated carbon with other low-cost carbon materials [4,14,38-46] is listed in Table 6, which shows that activated carbon derived from DRH had a relatively large adsorption capacity compared to some data obtained from the published literature.

Table 6. Comparing the adsorption capacity of activated carbon with other carbon materials

Raw material	Activated agent	Iodine adsorption capacity ($mg \cdot g^{-1}$)	MB adsorption capacity ($mg \cdot g^{-1}$)	Reference
Date stones	$FeCl_3$	761.40	255.32	[4]
Date palm pits	CO_2		110	[38]
Ramulus mori	$NH_4H_2PO_4$	847.21	314.1	[39]
Date pits	$FeCl_3$	761.40	259.25	[40]
Salsola vermiculata	$ZnCl_2$	1178	130	[41]
Sewage sludge	Steam	186.36	130.69	[42]
Olive bagasse	Steam	500		[14]
Albizia lebbeck seed pods	KOH		381.22	[43]
Black liquor lignin	Steam		92.51	[44]
Cotton stalk	$ZnCl_2$	972.92	193.50	[45]
Buriti shells	$ZnCl_2$	274.62		[46]
DRH	Steam	970.06	382.65	In study

4. Porosity and Pore Size Distribution

The BET surface area and porous properties of residue and activated carbon were determined from N_2 adsorption experiments. Microporous surface and external surface, as well as micropore volume were evaluated by *t*-plot method [47]. The mean pore diameter D_p, which was calculated from $D_P=4V_T/S$, V_T was the total volume of pores, and S was the BET surface area.

Fig. 7 shows an adsorption-desorption isotherm of N_2 at 77 K for activated carbon. From this figure, the volume adsorbed increases sharply at low relative pressure, which clearly indicates the existence of micropores. The adsorption capacity increases with increase of relative pressure up to a P/P_0 value of 1. The pore size distribution plot shown in Fig. 8 indicates that the pore volume and radius of activated carbon change rate, with average pore diameter estimated to be 2.043 nm. The surface area of activated carbon was estimated to be 1,004.296 $m^2 \cdot g^{-1}$, while total pore volume was 0.9388 $cm^3 \cdot g^{-1}$. The micropore volume of obtained activated carbon had 0.247 $cm^3 \cdot g^{-1}$ and micropore area was 568.829 $m^2 \cdot g^{-1}$ as a basis of *t*-plot method.

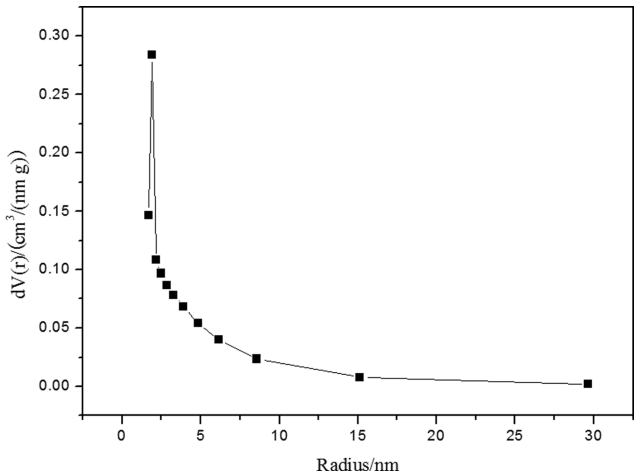

Fig. 8. The pore size distribution of the optimization activated carbon.

5. SEM and FTIR Analysis

Fig. 9 shows the scanning electron micrographs (JEOL 6335F-SEM, Japan) of DRH(a) and activated carbon(b). From Fig. 9(a), there are almost fewer pores on the surface of DRH. It can be seen from the Fig. 9(b) that the external surface of activated carbon has crevices and some pores in various sizes on the surface of acti-

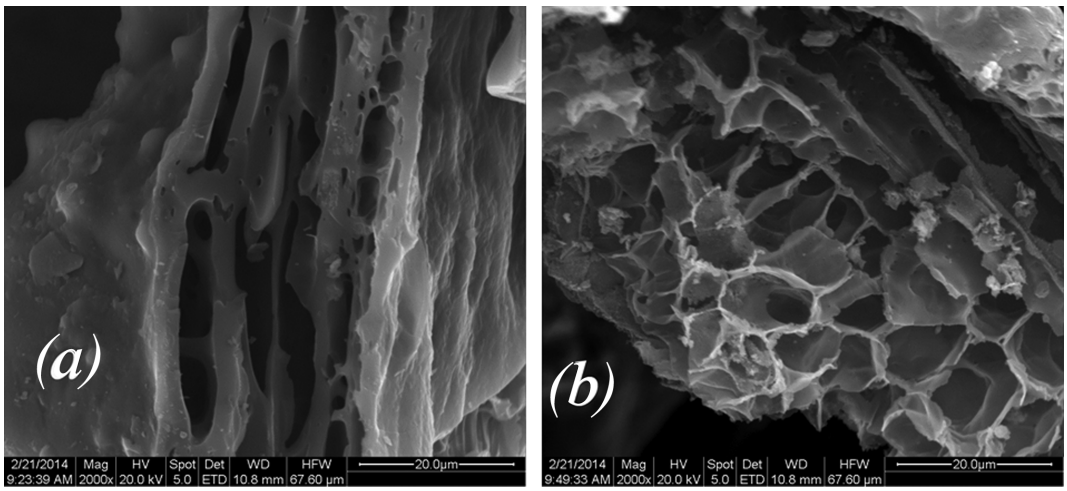

Fig. 9. The SEM micrograph of DRH (a) and activated carbon (b).

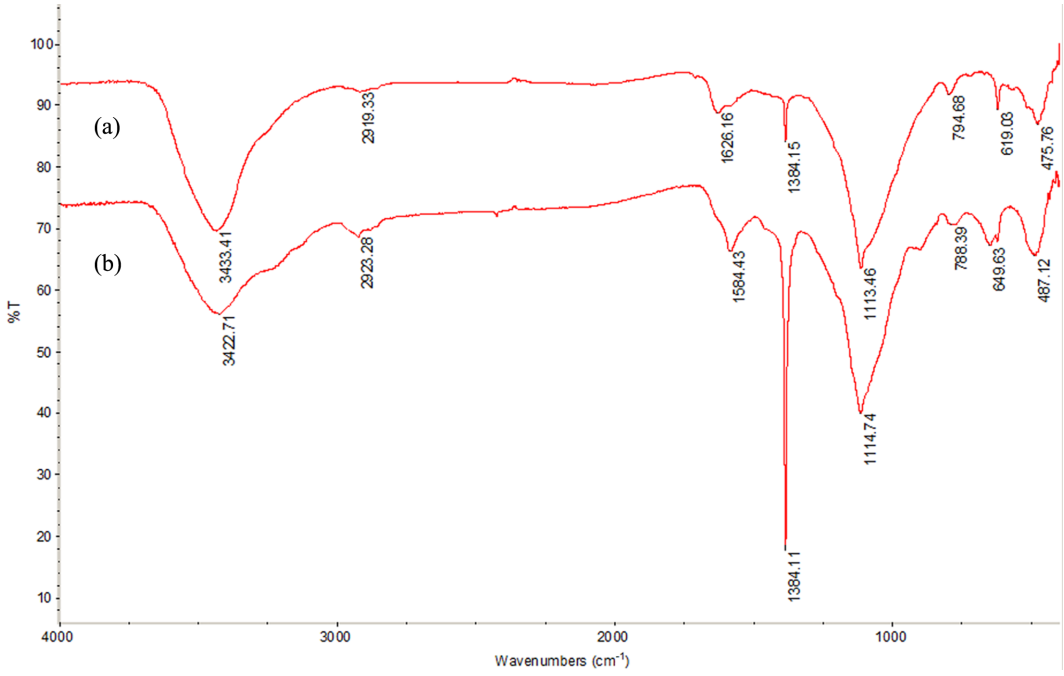

Fig. 10. The FTIR spectrum of DRH (a) and activated carbon (b).

vated carbon. SEM observation reported in Fig. 9 shows that these pores appeared because of activation with steam as activator at high temperature.

The functional groups present in DRH and activated carbon were characterized by a Fourier transform infrared spectrometer (PE-1710, USA), using potassium bromide discs to prepare the samples. The FTIR spectrum of DRH and activated carbon is shown in Fig. 10. The FTIR spectrum of DRH shows a broad band at 3,433.41 cm^{-1}, which is typically ascribed to O-H stretching vibrations mode of hydroxyl functional groups or adsorbed water. The peak at 2,919.33 cm^{-1} may be attributed to C-H stretching vibration of aliphatic carbon or can be due to $-CH_2$ or $-CH_3$ deformation [48]. The peak in the region of 1,626.16 cm^{-1} indicates the presence of C=O group stretching from ketones and aldehydes [49,50]. The peak at 1,384.15 cm^{-1} indicates the presence of primary amides and signifies N-H in-plane bending and C-N stretching. The peak around 1,384.15 cm^{-1} in DRH may also be due to the $-NO_2$ group symmetric stretching [50]. The peak at around 1,113.46 cm^{-1} band may be attributed to the Si-O-Si and -C-O-H stretching and -OH deformation [49]. The peaks at 794.68 cm^{-1} and 475.76 cm^{-1} indicate the presence of Si-H in the rice husk [49]. From Fig. 10(b), the characteristic function groups of activated carbon have changed; the peak changed to sharper than that in DRH around 1,384.11 cm^{-1} in activated carbon. The shifting occurs both to higher and lower wave numbers.

CONCLUSIONS

RSM was used to study effects of three activated carbon preparation variables-- activated temperature, activation time and amount of the steam--on iodine adsorption capacity. It was concluded that activation temperature showed the most significant effect on iodine adsorption capacity from the model, and the R^2 values of all parameters shown a good fit of model with experimental data. Through analysis of response surfaces derived from equation, the best optimization was an activation temperature of 946 °C, activation time of 31 min and 18 g of water. The optimum activated carbon showed iodine uptake of 970.06 $mg \cdot g^{-1}$, the activated carbon yield was 31.36% under these conditions. The BET specific surface area can be significantly enlarged by activation process up to 1,004.296 $m^2 \cdot g^{-1}$, and the average pore radius was about 2.043 nm, total pore volume of 0.9388 $cm^3 \cdot g^{-1}$. The micropore volume of obtained activated carbon had 0.247 $cm^3 \cdot g^{-1}$ and micropore area was 568.829 $m^2 \cdot g^{-1}$. The surface chemical functional groups of activated carbon were identified by FTIR, and its microstructure was examined by SEM; there were more pores than DRH due to steam activation. The results suggest that residue of rice husk can be used as raw materials for preparing activated carbon which has higher quality, and this process is harmless for the environment.

ACKNOWLEDGEMENTS

The authors express their sincere gratitude to the Center of Biology and Chemical Engineering and the State Key Laboratory of Motor Vehicle Biofuel Technology (Grand No. 2013007) for the financial support of this study.

REFERENCES

1. S. V. Mikhalovsky and V. G. Nikolaev, *Interface Sci.*, **7**, 529 (2006).
2. F. C. Wu, R. L. Tseng and C. C. Hu, *Micropor. Mesopor. Mater.*, **80**, 9 (2005).
3. A. Aworn, P. Thiravety and W. Nakbanpote, *J. Anal. Appl. Pyrolysis*, **82**, 279 (2008).
4. M. J. Ahmed and S. K. Theydan, *Powder Technol.*, **229**, 237 (2012).
5. R. H. Hesas, W. M. A. Wan Daud, J. N. Sahu and A. Arami-Niya, *J. Anal. Appl. Pyrolysis*, **100**, 1 (2013).

6. S. K. Ryu, H. Jin, D. Gondy and N. Pusset, *Carbon*, **5**, 31 (1993).
7. T. Wigmans, *Carbon*, **1**, 27 (1989).
8. S. M. Guillermo, D. F. Geoffrey and J. S. Christopher, *Carbon*, **41**, 1009 (2003).
9. C. F. Chang, C. Y. Chang and W. T. Tsai, *J. Colloid Interface Sci.*, **232**, 45 (2000).
10. B. H. Hameed, I. A. W. Tan and A. L. Ahmad, *J. Hazard. Mater.*, **158**, 324 (2008).
11. H. Y. Kang, S. S. Park and Y. S. Rim, *Korean J. Chem. Eng.*, **23**, 948 (2006).
12. Y. W. Zhu, J. H. Gao, Y. Li, F. Sun and Y. K. Qin, *Korean J. Chem. Eng.*, **28**, 2344 (2011).
13. M. F. Tennant and D. W. Mazyck, *Carbon*, **41**, 2195 (2003).
14. H. Demiral, İ. Demiral, B. Karabacakoğlu and F. Tümsek, *Chem. Eng. Res. Des.*, **89**, 206 (2011).
15. Y. Ngernyen, C. Tangsathitkulchai and M. Tangsathitkulchai, *Korean J. Chem. Eng.*, **23**, 1046 (2006).
16. C. A. Toles, W. E. Marshall, L. H. Wartelle and A. McAloon, *Bioresour. Technol.*, **75**, 197 (2000).
17. A. V. Esin and E. P. Ayşe, *J. Anal. Appl. Pyrolysis*, **98**, 29 (2012).
18. B. C. Kim, Y. H. Kim and T. Yamamoto, *Korean J. Chem. Eng.*, **25**, 5 (2008).
19. Z. Z. Chowdhury, S. M. Zain, R. A. Khan and Md. S. Islam, *Korean J. Chem. Eng.*, **29**, 1187 (2012).
20. P. Fu, S. Hu, J. Xiang, W. M. Yi, X. Y. Bai, L. S. Sun and S. Su, *Bioresour. Technol.*, **114**, 591 (2012).
21. C. Deiana, D. Granados, R. Venturini, A. Amaya, M. Sergio and N. Tancredi, *Ind. Eng. Chem. Res.*, **47**, 4754 (2008).
22. Y. Lin, Y. P. Guo, W. Gao, Z. Wang, Y. J. Ma and Z. C. Wang, *J. Clean Prod.*, **32**, 204 (2012).
23. A. A. M. Daifullah, B. S. Girgis, H. M. H. Gad, *Mater. Lett.*, **57**, 1723 (2003).
24. S. Román, J. F. González, C. M. González-García and F. Zarmora, *Fuel Process. Technol.*, **89**, 715 (2008).
25. J. Lee, L. Ye, W. O. Landen and R. R. Eitenmiller, *J. Food Compos. Anal.*, **13**, 45 (2000).
26. J. M. Valente Nabais, P. Nunes, P. J. M. Carrott, M. M. L. Ribeiro Carrott, A. Macías García and M. A. Díaz-Díez, *Fuel Process. Technol.*, **89**, 262 (2008).
27. M. A. Ahmad and R. Alrozi, *Chem. Eng. J.*, **165**, 883 (2010).
28. X. H. Duan, C. Srinivasakannan, W. W. Qu and X. Wang, *Chem. Eng. Process.*, **53**, 53 (2012).
29. A. A. Ahmad, B. H. Hameed and A. L. Ahmad, *J. Hazard. Mater.*, **170**, 612 (2009).
30. A. Arami-Niya, W. M. A. Wan Daud, F. S. Mjalli and F. Abnisa, *Chem. Eng. Res. Des.*, **90**, 776 (2012).
31. L. X. Huang, M. X. Wang, Y. P. Wu, L. R. Li and F. M. Zhou, *J. Nanjing Inst. Forestry*, **1**, 31 (1986).
32. A. Aranda, R. Murillo, T. García and A. M. Mastral, *Chem. Eng. J.*, **187**, 123 (2012).
33. Y. Sudaryanto, S. B. Hartono, W. Irawaty, H. Hindarso and S. Ismadji, *Bioresour. Technol.*, **97**, 734 (2006).
34. B. G. P. Kumar, K. Shivakamy, L. R. Miranda and M. Velan, *J. Hazard. Mater.*, **B136**, 922 (2006).
35. Ç. Şentorun-Shalaby, M. G. Uçak-Astarlıoğlu, L. Artok, Ç. Sarıcı, *Micropor. Mesopor. Mater.*, **88**, 126 (2006).
36. L. S. Balistrieri and J. W. Murray, *Am. J. Sci.*, **281**, 788 (1981).
37. P. Luo, B. Zhang, Y. Zhao, J. Wang, H. Zhang and J. Liu, *Korean J. Chem. Eng.*, **28**, 800 (2011).
38. K. S. Kumar Reddy, A. Al Shoaibi and C. Srinivasakannan, *New Carbon Mater.*, **27**, 344 (2012).
39. Y. B. Tang, Q. Liu and F. Y. Chen, *Chem. Eng. J.*, **203**, 19 (2013).
40. S. K. Theydan and M. J. Ahmed, *J. Anal. Appl. Pyrolysis*, **97**, 16 (2012).
41. B. Bestani, N. Benderdouche, B. Benstaali, M. Belhakem and A. Addou, *Bioresour. Technol.*, **99**, 8441 (2008).
42. W. H. Li, Q. Y. Yue, B. Y. Gao, X. J. Wang, Y. F. Qi, Y. Q. Zhao and Y. J. Li, *Desalination*, **278**, 179 (2011).
43. M. J. Ahmed and S. K. Theydan, *J. Anal. Appl. Pyrolysis*, **105**, 199 (2014).
44. K. F. Fu, Q. Y. Yue, B. Y. Gao, Y. Y. Sun and L. J. Zhu, *Chem. Eng. J.*, **228**, 1074 (2013).
45. H. Deng, L. Yang, G. H. Tao and J. L. Dai, *J. Hazard. Mater.*, **166**, 1514 (2009).
46. O. P. Jr. A. L. Cazetta, I. P. A. F. Souza, K. C. Bedin, A. C. Matins, T. L. Silva and V. C. Almeida, *J. Ind. Eng. Chem.*, JIEC-1895, No. pages 7 (2014).
47. N. Passe-Coutrin, S. Altenor, D. Cossement, C. Jean-Marius and S. Gaspared, *Micropor. Mesopor. Mater.*, **111**, 517 (2008).
48. Y. Chen, Y. C. Zhu, Z. C. Wang, Y. Li, L. L. Wang, L. L. Ding, X. Y. Gao, Y. J. Ma and Y. P. Guo, *Adv. Colloid Interface Sci.*, **163**, 39 (2011).
49. V. C. Srivastava, I. D. Mall and I. M. Mishra, *J. Hazard. Mater.*, **B134**, 257 (2006).
50. U. R. Lakshmi, V. C. Srivastava, I. D. Mall and D. H. Lataye, *J. Environ. Manage.*, **90**, 710 (2009).